TABLE 2

Surface Colour Gradients.

| Identification | T | $\frac{\Delta(B-V)_I}{\Delta\alpha}$ | $\frac{\Delta(B-V)_O}{\Delta\alpha}$ | $\frac{\Delta(B-R)_I}{\Delta\alpha}$ | $\frac{\Delta(B-R)_O}{\Delta\alpha}$ | $\frac{\Delta(V-R)_I}{\Delta\alpha}$ | $\frac{\Delta(V-R)_O}{\Delta\alpha}$ | Break |
|---|---|---|---|---|---|---|---|---|
| **Warm Seyfert 1** | | | | | | | | |
| 15015+1037 (359) | -5 | 0.074(5) | -0.014(4) | 0.178(12) | 0.012(0.3) | 0.069(6) | -0.003(0.1) | 4 |
| 23016+2221 (547) | -5 | 0.112(14) | 0.017(1) | 0.123(11) | 0.011(0.7) | -0.024(48) | -0.006(0.5) | 5.5 |
| 09497-0122 (260) | -3 | ··· | ··· | ··· | ··· | -0.024(0.6) | ··· | ··· |
| 02366-3101 ( 55) | 0 | 0.067(17) | 0.010(0.3) | 0.080(11) | 0.008(0.3) | 0.015(3)) | -0.002(0.1) | 4.8 |
| 04493-6441 (153) | 0 | ··· | ··· | 0.103(51) | 0.039(2) | 0.041(10) | 0.012(0.2) | 4 |
| 21299+0954 (521) | 0 | 0.082(3) | 0.005(0.1) | 0.063(4) | 0.002(0.1) | -0.020(5) | -0.002(0.3) | 8 |
| 00509+1225 ( 18) | 1 | 0.148(7) | 0.001(0.1) | 0.200(18) | -0.004(0.1) | 0.114(28) | -0.005(0.2) | 5 |
| 05136-0012 (171) | 2 | ··· | ··· | ··· | ··· | -0.006(0.5) | ··· | ··· |
| 04339-1028 (139) | 3 | ··· | ··· | 0.072(24) | 0.014(3) | ··· | ··· | 3 |
| 09453+5043 (259) | 3 | ··· | ··· | ··· | ··· | -0.035(4) | 0.014(0.9) | 5.5 |
| 14557-2830 (358) | 3 | ··· | ··· | ··· | ··· | 0.057(29) | -0.025(1) | 3 |
| 01378-2230 ( 31) | 10 | ··· | ··· | 0.108(12) | 0.008(0.3) | ··· | ··· | 7 |
| **Warm Seyfert 2** | | | | | | | | |
| 04507+0358 (156) | -4 | -0.029(0.5) | ··· | -0.036(0.7) | ··· | ··· | ··· | ··· |
| 00521-7054 ( 19) | -3 | ··· | ··· | -0.095(9) | -0.009(0.2) | ··· | ··· | 4 |
| 20481-5715 (512) | -1 | -0.015(15) | -0.016(1) | -0.029(10) | -0.027(2) | -0.013(4) | -0.007(0.8) | 4 |
| 03202-5150 ( 80) | -1 | ··· | ··· | -0.056(5) | 0.008(0.4) | 0.011(0.2) | ··· | 4 |
| 22017+0319 (528) | -1 | ··· | ··· | ··· | ··· | 0.056(9) | 0.001(0.1) | 4 |
| 03355+0104 ( 96) | 0 | ··· | ··· | 0.031(15) | 0.020(3) | ··· | ··· | 4 |
| 11298+5313W (283) | 0 | -0.087(17) | -0.195(16) | -0.119(7) | -0.249(18) | -0.044(5) | -0.054(8) | 3 |
| 02580-1136 ( 67) | 1 | ··· | ··· | -0.015(3) | -0.005(0.3) | -0.004(0.3) | ··· | 10 |
| 13144+4508 (315) | 1 | -0.030(0.6) | ··· | -0.121(13) | -0.029(0.6) | ··· | ··· | 4 |
| 00321-0019 ( 9) | 2 | ··· | ··· | ··· | ··· | -0.001(5) | -0.015(0.8) | 4 |
| 03059-2309 ( 72)* | 3 | -0.014(1) | 0.008(0.7) | -0.079(10) | 0.004(0.2) | -0.069(17) | -0.0003(0.2) | 4 |
| 11298+5313E (283) | 3 | -0.059(15) | -0.020(2) | ··· | ··· | ··· | ··· | 3.8 |
| 03362-1641 ( 98)* | 3 | ··· | ··· | -0.074(¿100) | -0.011(0.6) | ··· | ··· | 3.8 |
| 23254+0830 (555) | 4 | -0.068(23) | -0.001(0.1) | -0.089(30) | -0.012(1) | -0.021(14) | -0.006(2) | 4 |
| 13536+1836 (333) | 10 | -0.422(24) | -0.026(1) | -0.244(16) | -0.015(0.8) | 0.177(44) | 0.002(0.1) | 3.5 |
| 19254-7245 (489) | 10 | -0.051(17) | -0.008(0.5) | -0.136(23) | -0.017(0.8) | -0.087(15) | -0.008(0.4) | 3.9 |
| **Cold Sample** | | | | | | | | |
| 02439-7455 | -5 | ··· | ··· | 0.171(>100) | -0.002(0.1) | ··· | ··· | 3.5 |
| 04015-1118 | 1 | ··· | ··· | 0.106(13) | -0.005(0.6) | ··· | ··· | 3 |
| 23179-6929 | 1 | ··· | ··· | ··· | ··· | -0.061(70) | -0.027(1) | 3 |
| 05207-2727 | 2 | ··· | ··· | -0.097(14) | -0.001(0.2) | ··· | ··· | 3.7 |
| 09406+1018N | 2 | ··· | ··· | -0.110(69) | -0.035(0.4) | ··· | ··· | 3 |
| 07514+5327 (231) | 3 | -0.050(3) | -0.005(0.3) | ··· | ··· | ··· | ··· | 4.5 |
| 10475+1429W | 3 | ··· | ··· | -0.045(13) | -0.019(0.8) | ··· | ··· | 4 |
| 04304-5323 | 3 | ··· | ··· | ··· | ··· | -0.020(8) | 0.001(0.1) | 8 |
| 06506+5025 (211) | 5 | 0.053(4) | ··· | -0.001(0.1) | ··· | -0.054(9) | ··· | ··· |
| 05217-4245* | 5 | ··· | ··· | -0.058(58) | 0.0(¡0.1) | ··· | ··· | 3.5 |
| 04265-4801 | 5 | ··· | ··· | -0.017(2) | ··· | ··· | ··· | ··· |

TABLE 2—*Continued*

| Identification | T | $\frac{\Delta(B-V)_I}{\Delta\alpha}$ | $\frac{\Delta(B-V)_O}{\Delta\alpha}$ | $\frac{\Delta(B-R)_I}{\Delta\alpha}$ | $\frac{\Delta(B-R)_O}{\Delta\alpha}$ | $\frac{\Delta(V-R)_I}{\Delta\alpha}$ | $\frac{\Delta(V-R)_O}{\Delta\alpha}$ | Break |
|---|---|---|---|---|---|---|---|---|

NOTE.—The subscripts $I$ and $O$ indicate inner and outer colour gradients, as defined in the text

NOTE.—The distance indicating the *Break* in the colour profiles is expressed in kpc

NOTE.—The values inside parentheses indicate the goodness for each estimated coefficient in terms of multiple of the associated $\sigma$ values

NOTE.—Objects indicated with * show an intermediate region in $(B-R)$ profiles, with slopes: 03059-2309: -0.014, 03362-1641:-0.034 and 05217-4245: -0.026

# Multicolour Optical Imaging of IR-Warm Seyfert Galaxies. IV. Surface Photometry: Colour Distributions

Eleni T. Chatzichristou
*Leiden Observatory, P.O. Box 9513, 2300 RA Leiden, The Netherlands*
*NASA/Goddard Space Flight Center, Code 681, Greenbelt, MD 20771*

## ABSTRACT

This paper is the fourth in a series, studying the optical properties of a sample of mid-IR Warm Seyfert galaxies and of a control sample of mid-IR cold galaxies. The present paper is devoted to the analysis of the colour distributions characterizing the host galaxies. The Warm Seyfert 1 and 2 galaxies show opposite colour gradients and their colour profiles are depicting age and dust effects within single-burst, solar metallicity models. In particular, we find ample evidence for the occurrence of strong star formation in the Seyfert 2 disks: their colour and emission line two-dimensional maps suggest dust extinction associated with on-going star formation in spiral and tidal features; their colour profiles show starbursts of 0.5-1 Gyr or younger, superposed on the older underlying galaxy population. Most of these properties are shared with the Cold galaxies, while the Warm Seyfert 1s show mostly older stellar populations and, in only a few cases, evidence for circumnuclear star formation.

*Subject headings:* galaxies: active, Seyfert, interactions, photometry

## 1. Introduction

The present paper is devoted to the analysis of the optical colour distributions in a subsample of 54 mid-IR Warm Seyferts selected from the original sample of IR-warm IRAS sources of De Grijp et al. (1987 and 1992). This is compared to a control sample of 16 mid-IR cold IRAS galaxies, selected to span similar redshift and luminosity ranges as the Warm sample. In Chatzichristou 2000a (hereafter Paper I) we presented our optical imaging data. In Chatzichristou 2000b (hereafter Paper II) we discussed and intercompared the optical properties of these samples, resulting from aperture photometry. In Chatzichristou 2000c (hereafter Paper III) we parametrized the bulge and disk components of their host galaxies. In the present paper, we present and discuss extensively the colour distributions and their implications for the stellar and dust content of IR-warm Seyferts, in terms of 2D colour maps, radial colour gradients and colour-colour plots, in Sections 2, 3 and 4, respectively. In Section 5 we summarize our conclusions. We also refer the reader to the Appendix of Paper III. where we presented radial colour profiles, colour-colour plots and 2D colour and emission line maps, together with a brief description, for each individual galaxy.

## 2. Colour and Emission-Line Maps

### 2.1. Presentation of Data

In the Appendix of Paper III we presented two dimensional colour maps for most of our sample objects. These were constructed after: (i) correcting the individual band images for geometrical distortion and aligning them, (ii) degrading the images to match the resolution of those with the worst seeing (the seeing for each image, as measured from field stars, is given in Tables 4 and 5 of Paper I), (iii) applying a "reasonable" noise cutoff ($\sim 2\sigma$) to all individual images before constructing the colour maps (iv) using the appropriate calibration formulas (the same used for the aperture magnitudes in Paper II) for each observing session, (v) convolving with a circular Gaussian function of $\sigma$=0.5 pix, to produce the smooth images shown in the Appendix.

The grey scales in most colour images range from 0-2 mags, except for the Seyfert 1s IRAS 01378-2230 and 04339-1028, the Seyfert 2 IRAS 03230-5800 and the Cold galaxy IRAS 23128-5919. These are objects with no available photometric calibration, for which surface magnitudes and colours have been estimated using a reasonable assumption for the mean galaxy colours (based on the other sample objects), but we do not include these estimated quantities in the quantitative analysis presented below. For the objects for which no colour maps are shown, this is either because they were too noisy (original images shallow) or because we have data only in one band.

When H$\alpha$ narrow band images are available, they are shown next to the colour maps. The H$\alpha$ images were produced by: (i) subtracting the background and aligning them with the broad band images, (ii) using the latter to estimate and subtract the continuum. The best result is judged by the smooth residuals in the resulting (continuum subtracted) image, everywhere in the galaxy except for the line emitting regions. The narrow band images are not flux calibrated, thus we used them to make qualitative morphological comparisons with the colour maps but cannot extract H$\alpha$ luminosities.

### 2.2. Results

We summarize here the qualitative conclusions drawn from inspection of the two-dimensional colour and emission line maps presented in the Appendix of Paper III.

Seyfert 1s: Their colour maps are mostly featureless. Almost all of them have blue central regions and colour gradients that become more positive (redder) outwards. Exceptions are (i) IRAS 14557-2830, a strongly interacting system with patchy red central regions and (ii) IRAS 23016+2221 and 04339-1028, both showing structure in their colour distributions associated with individual morphological peculiarities. We have only two Seyfert 1s with available H$\alpha$ maps: the line emission follows roughly the continuum light emission and is mainly centrally concentrated and/or delineates knotty spiral arms.

Seyfert 2s: Most galaxies have redder central regions with negative (bluer) colour gradients outwards. The colour distributions are more complex than in the case of Seyfert 1s: (a) In many cases narrow red features are seen as (i) one-sided red strips (*e.g.,* IRAS 04507+0358 and 20481-5715), (ii) lanes associated with inter-arm regions (*e.g.,* IRAS 23254+0830), edge-on disks (*e.g.,* IRAS 11298+5313E), or central bars (*e.g.,* IRAS 02580-1136 and 03059-2309). These features are most probably due to dust extinction or, when associated with a bar, to an older stel-

lar population. (b) Blue bright emission knots are observed, associated with spiral arms (*e.g.,* IRAS 02580-1136, 03059-2309, 23254+0830) or ring structures (*e.g.,* IRAS 03202-5150). These blue features are likely to be star forming regions, as seen by comparison of the colour and H$\alpha$ emission line maps. (c) There are two double nucleus merger products in our Seyfert 2 sample (IRAS 13536+1836 and 19254-7245) that show remarkably similar colour and line emission distributions: (i) the brightest of the two nuclei is also much redder; (ii) the line emission is centered on that nucleus and shows a spike-like emission feature perpendicular to the line connecting the two nuclei; (iii) blue knotty arms are seen in both these galaxies, probably associated with intense star formation. The detailed spectroscopic analysis and mapping of IRAS 13536+1836 extended emission-line region (Chatzichristou & Vanderriest 1995) have shown that the brighter/redder is also the Seyfert nucleus and that the gas is anisotropically ionized by the AGN. We suspect that this must also be the case for IRAS 19254-7245, given the similarity of features between the two objects.

(3) Cold galaxies: The vast majority of the Cold sample galaxies are strongly interacting systems, with complex morphologies and colour distributions: (i) Blue regions are associated with circumnuclear rings, (knotty) spiral arms, tidal loops and disk distortions, most probably indicating strong star formation events. (ii) Red features are irregular and patchy, or appear as one-sided lanes, associated with bars and edge-on disks. They most probably are due to a combination of dust effects and redder stellar populations, as in the case of Seyfert 2s. (iii) There is one double nucleus merger in our Cold sample (IRAS 23128-5919) that shows strikingly similar characteristics to the Warm Seyfert 2 mergers: the brighter and redder of the two nuclei in continuum light is also brighter in H$\alpha$ light and the line emission shows a spike perpendicular to the line connecting the two nuclei. It is interesting that this object is spectroscopically classified as a Seyfert 2.

We have observed an additional double nucleus system, the Seyfert 1 IRAS 19580-1818, not presented here because of its low S/N broad and narrow band images (a broad-band contour map is shown in Paper I). Its continuum and emission line characteristics are again strikingly similar to the ones described above for the Seyfert 2 and Cold merger systems.

## 3. Radial Colour Profiles and Colour Gradients

In the Appendix of Paper III, we have presented the (azimuthally averaged) radial colour profiles of our objects, constructed using surface magnitudes (corrected for Galactic absorption and K-correction). Consequently, labels such as $(B-V)$ signify $\mu_B - \mu_V$. The error bars are derived from the surface magnitude errors and are representative of the photometric uncertainties, except in the outer regions where uncertainties in the sky subtraction dominate (for details see Chatzichristou 1999). To avoid the noisy outer regions, we plotted radial colour profiles out to $\mu_B$=25 mag arcsec$^{-2}$. The horizontal axis is in linear scale and units of kpc and represents the galaxy's semi-major axis lengths. The inner cut-off in the profiles is applied to avoid seeing effects and is approximately equal to the seeing radius, as measured on the field stars. In what follows we will be discussing these data in terms of surface colour gradients and colour-colour plots. But first, we will summarize our results from the aperture colour gradients.

### 3.1. Aperture Colour Gradients

We use the nuclear (within a 2 kpc radius) and disk (between 2 kpc and the isophote corresponding to $\mu_B$=25 mag arcsec$^{-2}$) aperture colours from Paper II, in which we have also presented the colour distributions and colour correlations for each sample. We define the aperture colour gradients simply as

$$\Delta(Colour) = Colour_{(Disk)} - Colour_{(Nucleus)}$$

. Thus, a positive/negative colour gradient corresponds to a redder/bluer disk compared to the central 2 kpc region. In Figure 1 we plot the distributions of colour gradients and in Figure 2 the gradients as a function of host morphological type T, for our three (sub)samples. The corresponding median, mean and standard deviations are given in Table 1.

We summarize our main conclusions:

(i) Seyfert type 1 and 2 galaxies show opposite colour gradients (positive-negative, respectively). This was already noticed by us in Paper II, as well as, from the 2D colour maps and the radial colour profiles presented in the Appendix of Paper III. The distribution of $(V-R)$ gradients is narrower compared to the other colours and peaks around zero. This is likely a combined effect of (a) the short wavelength range, (b) the contamination of the $R$-band magnitudes (nuclear in

the case of Seyfert 1, disk in the case of Seyfert 2 and Cold galaxies) by H$\alpha$ emission and (c) the contamination of the $V$-band magnitudes by [O III]$_{4959,5007}$ emission. Seyfert 1s show positive gradients for all colours, $(B-V)$, $(B-R)$, $(V-I)$, which are most likely due to the presence of a "naked" AGN in their centers, that bluens significantly their nuclear colours (see also Figure 2 of Paper II). The negative colour gradients in Seyfert 2s are comparable to those found in normal galaxies, for which stellar population age and metallicity effects are the main contributors (De Jong 1996). In Seyfert 2s, reddening of the central regions due to dust obscuration could further steepen their colour gradients. Supporting evidence to the latter is the progressive flattening (less negative) of the colour gradients towards longer wavelengths.

(ii) The Cold sample galaxies all show negative outwards colour gradients. They are less steep than the Seyfert 2 gradients and are comparable for the $(B-R)$ and $(V-R)$ colours. These two facts are likely indicating that dust extinction and star formation are more evenly distributed throughout these objects.

(iii) There is no well-defined correlation between colour gradients and morphological type (with perhaps the exception of the Seyfert 2 $(V-I)$ gradients). The lack of correlation with morphological type for the Warm Seyferts, most likely indicates that the aperture colour gradients are affected by both the AGN and dust extinction, rather than simply reflecting stellar age and metallicity gradients. Morphological missclassifications, due to the complex host morphologies, is another likely reason for the lack of correlations with T, in particular for the highly disturbed, interacting Cold sample galaxies.

### 3.2. Surface Colour Gradients

#### *3.2.1. Definitions*

We used the isophotal fitting results from Paper III, to derive colours at each radius from the azimuthally averaged isophotal magnitudes. We are mainly interested in isolating the host colour gradients, thus we only use the data for radii larger than 2 kpc out to the $\mu_B$=25 mag arcsec$^{-2}$. For elliptical galaxies, it is common to plot radial colour profiles versus log radius because these are essentially linear functions. However, this is not the case for our objects and thus we choose to represent colour gradients in linear radius space. We then derived the colour gradients $\frac{\Delta(Colour)}{\Delta\alpha}$ from the slope of the radial colour profiles. Here $\alpha$ represents the semi-major axis length and *Colour* the surface colour. In this way, we measured colour gradients through weighted least-square fitting of a first-order polynomial, using the surface photometry errors to weigh the data. Inspection of the colour profiles in the Appendix of Paper III, shows that there is almost always a break in the profiles, particularly well-defined in the case of Seyfert 1s. We thus decided to fit most colour profiles in two regions, *inner* and *outer* from the break location, which is defined to be the point where the inner (linear) gradient stops fitting the data points. The outer portion of the profile is then fitted from the larger radii inwards. The gradients obtained in this way, are presented in Table 1 (subscripts $I$ and $O$ for the inner/outer gradients, respectively) and in Figures 3 - 5 (subscripts *in* and *out*). Defining the break point from the inner fits has the advantage that is less affected by the presence of structure in the galactic disks. The break radius (in kpc) is also listed in Table 1. When only one line is fitted to the totality of the profile, this is considered as *outer* disk gradient. The median, mean and standard deviations of the colour gradient distributions are listed in Table 3. The uncertainties in the calculated gradients are comparable for the different samples and for the various colours. The median errors are: 0.008 for $\frac{\Delta(B-V)_I}{\Delta\alpha}$ and $\frac{\Delta(B-R)_I}{\Delta\alpha}$, 0.004 for $\frac{\Delta(V-R)_I}{\Delta\alpha}$, 0.017 for $\frac{\Delta(B-V)_O}{\Delta\alpha}$ and $\frac{\Delta(B-R)_O}{\Delta\alpha}$ and 0.019 for $\frac{\Delta(V-R)_O}{\Delta\alpha}$. The errors in the outer gradients are larger by a factor of $\sim$10, due to the presence of structure in the disks and to sky subtraction uncertainties. Comparison of the median errors quoted above and the values listed in Tables 1 and 3, indicates that the inner $(B-V)$ and $(B-R)$ gradients are well defined (with errors at the $\sim$10% level or less), while the inner $(V-R)$ and all the outer gradients are very small (flat colour profiles), comparable to their associated errors.

#### *3.2.2. Results*

(i) All surface colour gradients are flatter (inner gradients are flatter by factors of 2 to 5) compared to the integrated ones, the former being less affected by nuclear light and thus more representative of the true disk gradients. This effect is more noticeable in Seyfert 2s. However, there still remains a pronounced difference between the Seyfert 1 and Seyfert 2 inner gradients, the former being always positive the latter

mostly negative. If the persistent inverse gradients in Seyfert 1s are due to contamination by nuclear light, this would mean that the AGN dominates the light at least inside the central 5 kpc (median break radius) in these objects. However, as we have shown in Paper III, it is very unlikely that the bulge component (resulting from our profile decomposition) in Seyfert 1s is contaminated by the AGN light. The outer disk gradients are distributed in a much narrower range around zero, but the distinction between the two Seyfert samples persists, the Seyfert 1s showing positive gradients even in the outer disk portion. Since no positive metallicity gradients are predicted by galaxy formation theories, these are likely to be age gradients, the younger stars being more centrally concentrated. The Student's T and the K-S tests show that the Seyfert 1 and 2 subsamples have statistically different inner *and* outer $(B-R)$ colour gradients (statistical significance better than 98%). We have checked for possible inclination effects, but we find no correlation between surface colour gradients and ellipticity for any of our samples. This is important, in particular for the Seyfert 2s, indicating that the host colour gradients are not dominated by orientation effects (and thus dust extinction).

The Cold sample surface colour gradients are also flatter than their integrated gradients (factor of $\leq$2) and are mostly overlapping with the Seyfert 2 gradients (Figures 4 and 5. The similarity between these two samples, noticed earlier for their disk luminosities, sizes and colours (Paper II), is likely to indicate that similar processes dominate the formation of their disks.

(ii) No correlation was found between surface colour gradients and morphological type for any of our samples. If the profile break is indicative of bulge/disk dominance, there should be a correlation between break radius and morphological type, but we find no such obvious correlation. On the contrary, for Seyfert 2 and Cold galaxies we find a very narrow range of break values (lower right panel of Figure 6), that is remarkably similar for the two (sub)samples, peaking around 3.5-4 kpc (with a dispersion of $\sim$1.5). The break radius distribution for Seyfert 1s is flatter and has a larger median $\sim$5 kpc. Modeling of the colour gradients of elliptical galaxies has shown that condensed dust distribution can produce a similar break in the colour profiles, marking the transition between optically thick and thin material. The location of this break provides then useful constraints on the extent and mass of the dust within a galaxy (Wise & Silva 1996). Our data show that this effect is likely to be more important in the case of Seyfert 2 (and possibly Cold) galaxies.

(iii) Next, we investigated the change in slope at the break point. In Figure 6 we plot inner versus outer surface colour gradients, the long-dashed line indicating the loci of equal gradients. Points to the right/left side of this line indicate steeper (more positive/negative, respectively) *inner* gradients. The furthest the points lie from this line the largest is the change in slope between the inner and outer parts of the colour profiles. First of all, we notice that there are no objects for which the *sign* of the slope changes between the inner and outer disk regions (upper left or lower right quarters of each plot). Seyfert 1s have typically steeper inner gradients (that is, more dramatic changes in slope at the break point) than Seyfert 2s. The detached point representing a Seyfert 2 galaxy with the most negative $(B-V)$ and $(B-R)$ and positive $(V-R)$ inner gradients is the double nucleus merger IRAS 13536+1836; its extreme colour gradients are due to the light contamination by the two nuclei, at $\alpha$=2 kpc. The other extreme Seyfert 2 galaxy, showing very blue outer colour gradients is IRAS 11298+5313W, the western member of a triple interacting system and one of the possible candidates for the associated IRAS source. Its distinct position from the rest of the sample might be indicating that it does not belong to the IRAS Warm sample (the E member of the triple system is the most probable IRAS candidate).

(iv) We now address the question of whether any correlations exist between the colour gradients and the optical or IR luminosities. There is a well-known difference in colour gradients (excluding dust effects) between bright and faint bulges of ellipticals and early type galaxies, that are clues to different formation mechanisms for these galaxies (Balcells & Peletier 1994). In fact, this dichotomy in colour gradients with absolute magnitude seems to persist even outside their central regions (Vader etal. 1998). In Figure 7 we show plots of colour gradients versus luminosities, for our data. We find no correlation between optical or IR luminosities and colour gradients for Seyfert 1s, but we do see a correlation between inner $(B-R)$ gradients and IR luminosities (both $L_{25}$ and $L_{FIR}$) for Seyfert 2s, in the sense of bluer gradients at larger IR luminosities. In fact, these correlations become very tight if we exclude the two points deviating towards

steeper gradients, that represent the galaxies IRAS 13536+1836 and 11298+5313W mentioned earlier to have unusually steep gradients compared to the rest of the sample. A Spearman Rank or a Kendall's Tau non-parametric test for the significance of the correlations give 0.02 for $\frac{\Delta(B-R)_I}{\Delta\alpha}$ vs $L_{25}$ and 0.007 for $\frac{\Delta(B-R)_I}{\Delta\alpha}$ vs $L_{FIR}$. A similar trend is seen, for the inner $(B-R)$ gradients to correlate with $L_{FIR}$ for the Cold sample, but the data points are fewer and the scatter larger (correlation significance 0.04).

There are two possible ways to interpret the tight correlation seen for Seyfert 2s, given that the IR luminosity scales with the amount of (warm) dust within a galaxy: (a) if the dust is concentrated in the central regions, we expect negative (outwards) colour gradients that are steeper the larger is the effect of dust reddening in the center (b) if the warm dust is distributed throughout the disk, larger IR luminosities indicate a stronger source of illumination, most probably strong disk star formation that also causes the optical colours to bluen outwards. If alternative (a) is correct, then we would expect that a fair amount of dust heating in the center would be due to the AGN and thus the above correlation would be better defined versus $L_{25}$. Alternative (b) on the other hand, would be better represented by the correlation versus $L_{FIR}$. In fact, since both correlations are observed, the most probable explanation is a combination of the two effects.

(v) To seek an explanation for the above correlations, we inspected the continuum images (Paper I) and colour maps (Appendix of Paper III) for our Seyfert 2 sample. We find a clear correlation between increasing interaction strength and larger IR luminosities or steeper colour gradients. This result can be understood if strong interactions bring larger amounts of gas and dust to the center, induce strong star formation events throughout the disk and in the central regions and maybe feed the AGN, thus increasing the level of nuclear activity. Bushouse & Werner 1990 have also noticed larger scale and steeper optical and near-IR colour gradients in interacting and star-forming galaxies, compared to normal spirals. This result will be explored in more detail in Paper V.

### *3.2.3. Discussion*

Having explored the colour distributions and radial gradients for our sample galaxies, we compare now our data to normal galaxies and other Seyfert samples. Elliptical and early type galaxies are evolved systems, almost entirely composed by old red stars. Colour gradients in these galaxies are always negative outwards and can mostly be explained by metallicity effects. This is probably also the case for the bulges of early type spirals, although their colours are in general bluer than ellipticals, indicating that the bulge stellar populations are younger and/or more metal poor (Balcells & Peletier 1994). Moreover, their colour gradients do not seem to correlate with galaxy type (which is also what we found for the inner gradients of our sample galaxies). Negative colour gradients are also typical for intermediate and late type spirals. Here, many other effects are present besides metallicity gradients: variable internal extinction, dust re-radiation and the distribution of different stellar population types, can all influence the observed (bulge and disk) colours and gradients (*e.g.,* Bell & De Jong 1999, De Jong 1996). It is clear that the behaviour of our Warm Seyfert 2 and Cold galaxies is closer to that observed for normal spirals, the former having steeper colour gradients than the latter, indicating that dust effects in their central regions are important. Although the integrated colour gradients of Seyfert 1s are influenced by the presence of the AGN in their centers, it is not clear why the inverse (positive outwards) gradients persist also outside the central 2 kpc region (surface colour gradients). Positive gradients, when found in dwarf ellipticals, are interpreted as stellar age gradients: the evolution in these objects is dominated by internal processes, such as galactic winds and dissipation, that prevent the formation of metallicity gradients in these objects (Vader etal. 1998).

The differing colour properties of the disks of Warm Seyfert 1 and 2 galaxies are likely to be intrinsic and thus difficult to reconcile with a simple orientation effect. There is little information in the recent literature about Seyfert colour gradients. Kotilainen & Ward 1994 computed optical and near-IR *aperture* colour gradients for a sample of hard X-ray selected, mainly Seyfert 1 galaxies. After subtracting the AGN contributions they find negative optical and IR gradients, comparable to those of normal galaxies and certainly smaller than those found in interacting and starburst galaxies. They give $\Delta(B-V)$=-0.07 which is comparable to the inner surface colour gradients that we found for our Seyfert 2 sample. In fact, MacKenty 1990 has found redder disks than nuclei for his sample of Markarian and NGC Seyferts, in par-

ticular for objects with amorphous or peculiar morphologies (see also Figure 9). The range of his colours and medians are comparable to our results for the IR Warm Seyferts. We computed the mean *integrated* (Disk-Nucleus) colour gradients for MacKenty's data and find mean $(B-V)$=0.14, $(B-R)$=0.09, $(V-R)$:-0.05. These are comparable with our data for the Warm Seyfert 1 aperture colour gradients (Table 1). However, MacKenty's definition of nuclear and total aperture colours is different than ours, which makes this comparison less meaningful.

It is difficult to quantitatively interpret our results, given the multiplicity of factors that can affect the colours within a galaxy. Colour gradients that are primarily due to dust extinction are positive inwards at any given wavelength, but their morphology and magnitude will depend on the amount and distribution of the dust. Assuming some given dust properties, the colour gradients should then have similar overall morphologies at all wavelengths, but the slopes will be much steeper at shorter wavelengths (larger optical depths). Moreover, because these slopes are likely to be strongly affected by stellar population (age and metallicity) gradients as well, the latter effects are better explored in the near-IR where colour gradients are more insensitive to dust. Without such near-IR data it is impossible to discriminate between stellar population and dust as sources of the observed optical colour gradients. Even with near-IR data, metallicity and extinction could still be degenerate and other types of data, such as high resolution spectra and/or resolved images redwards of the near-IR, are necessary to settle the question unambiguously.

## 4. Stellar Populations

Many systematic studies of star formation rates (SFR) in spiral galaxies show that the variation of optical colours and H$\alpha$ properties through the Hubble sequence is due to different birthrate histories in the galactic disks: early type (S0-Sb) galaxies formed most of their stars in less than $t_{Hubble}$, but late type systems (Sc-Irr) form stars in a constant rate since their birth and will continue to form stars for several Gyr (*e.g.,* Kennicutt etal. 1994 and references therein). Modeling of the broad band colours is a very useful tool in this respect, providing that one uses disk colours that are unaffected by the old spheroidal component, rather than integrated colours. This approach was used by a number of workers, in order to study normal galaxies. Kennicutt etal. 1994 and Devereux & Young 1991 suggested that changes in photometric properties along the Hubble sequence are purely due to the evolutionary (star formation) history of disks and nearly independent of the changing $B/D$ ratio. Kennicutt etal. 1994 found that the observed properties of disks involve an initial mass function (IMF) which is enriched in massive stars by factors 2-3 over the solar neighborhood IMFs of Miller & Scalo 1979 and Scalo 1986. He also found that a finite-time recycling of the gas (returned from stars or/and through interactions) increases the life-time of the gas up to 5-15 Gyr (compared to 3 Gyr for instantaneous recycling). An important conclusion reached by Kennicutt was that the disk SFR per unit luminosity changes dramatically through the Hubble sequence (0.01-0.1 in Sa-Sb, 0.5-2 in Sc), while this change is much smaller within individual disks. The opposite however was found to be true for the (mean and radial respectively) disk surface densities. These two findings suggest that what determines the SFR in galactic disks is not merely the local gas surface density. De Jong 1996 found for his sample of face-on spirals, that their radial colour gradients are matched by differences in the star formation *histories* (SFH) within a galaxy. The outer parts are populated by young stars, while the red colours of the central regions require a range of metallicities in a relatively old stellar population. Bell & De Jong 1999 have reached a different conclusion than Kennicutt etal. 1994, suggesting that, in spiral galaxies, the local surface density is the most important parameter in determining the star formation history and together with the galaxy mass, the galaxy's chemical evolution.

In this section we are going to investigate the stellar population content of our sample galaxies, based on their IR properties and our optical photometry results.

### 4.1. Star Formation Rates

Optical and IR luminosities measure star formation over slightly different time periods: the H$\alpha$ emission is mainly due to ionization by young stars ($\leq 10^7$yr) while the IR luminosity is a measure of star formation over the past $10^8$-$10^9$yr. We have calculated approximate SFRs for our objects, based on their far-IR ($\geq$60 $\mu$m) luminosities. We use the standard formula $SFR_{IR} = 1.3 \times 10^{-43} L_{FIR} M_{\odot} yr^{-1}$ ($L_{FIR}$ in ergs cm$^{-2}$ sec$^{-1}$), adopted from Hunter etal. 1986, for a Salpeter IMF (Salpeter 1955) between 0.1-

100 $M_{\odot}$. Although IR luminous galaxies seem to require a larger IMF (*e.g.,* Rieke etal. 1980, Rieke etal. 1993), this is more complicated to assess than in the case of normal galaxies, because of the heavy obscuration in those systems and the highly time-variable SFRs. The conventional IMF chosen here is sufficient to make an inter-comparison of our samples.

In Figure 8 we plot the histograms of $\mathrm{SFR}_{IR}$ for our three subsamples and their median values as vertical bars. All samples span a large range of SFRs, in particular the Cold sample (9-380 $M_{\odot}\mathrm{yr}^{-1}$) which has a larger median 71.5 $M_{\odot}\mathrm{yr}^{-1}$ than the Warm sample. The Seyfert 1 and Seyfert 2 subsamples span similar ranges ($\sim$5-150) with medians 24.9 and 38.6 $M_{\odot}\mathrm{yr}^{-1}$ respectively, excluding the four highly IR luminous ($L_{60} \geq 10^{11}$) Seyfert 2s that have $\mathrm{SFR}_{IR} \geq 150$ $M_{\odot}\mathrm{yr}^{-1}$. When the four ultraluminous (UL) objects are included the two samples have significantly different variances and means (significance 0.0001 and 0.02, respectively).

We should be cautious when interpreting the FIR luminosities as reliable indicator of the star formation activity in galaxies. It is important to compare samples for which the (precursor) galaxy dust properties are known and similar. For instance, there is very likely an intrinsic difference in the dust content of galaxies selected at 60 $\mu$m, compared to galaxies selected optically. Also, bigger galaxies reradiate more energy at all wavelengths (ideally one should normalize $L_{FIR}$ by the galaxy size). Moreover, $L_{FIR}$ is due to different dust components, only the warmer component being associated with star formation. However, in dusty star forming regions with large optical depth, the stellar radiation field is dominated by young stellar populations and thus $L_{FIR}$ effectively measures the $L_{bol}$ of the starburst. Moreover, in Paper II we have shown that the $L_{FIR}$ for our samples is related to the disk component, thus it is less dependent on the AGN. Consequently, the assumption of $L_{FIR}$ being an accurate star formation indicator seems to be a good approximation for the objects in our (IR-selected) samples. Keeping in mind the limitations outlined above, it is instructive to compare our results with those of some other characteristic galaxy samples. Using the equivalent widths of H$\alpha$ emission, Kennicutt 1983 found a SFR (extinction corrected) as high as 20 $M_{\odot}\mathrm{yr}^{-1}$ in giant Sc galaxies and suggested that in late-type spirals, current SFRs are similar to past SFRs averaged over the age of the disk. SFRs obtained from IR data are usually larger than those from optical emission; Armus etal. 1990 argued that a factor of $\sim$3 difference between the two values is within the uncertainties attached to the models used for the calculation of SFRs and to the poorly known amount of extinction that affects the H$\alpha$ emission. For a sample of isolated galaxies, drawn from the complete IRAS bright galaxy sample (with $f_{60} \geq$5.24 Jy) the mean $\mathrm{SFR}_{IR}$ is 9.9 $M_{\odot}\mathrm{yr}^{-1}$ (Soifer etal. 1989). A sample of Markarian on-going and advanced merging systems (most of them starbursts and some Seyferts) shows median $\mathrm{SFR}_{H\alpha}$=6.8 $M_{\odot}\mathrm{yr}^{-1}$ and $\mathrm{SFR}_{IR}$=12.5 $M_{\odot}\mathrm{yr}^{-1}$ (Mazzarella etal. 1991). In these multiple-nucleus systems, warm dust is concentrated in the nuclear regions and is heated by active star formation, producing the bulk of far-IR emission and their warm far-IR colours. It is clear that our IR-warm Seyfert samples show larger values than their Markarian (UV-selected) counterparts. A far-IR warm (colour-selected) sample of powerful FIR galaxies (Armus etal. 1990) shows mean $\mathrm{SFR}_{H\alpha}$=40 $M_{\odot}\mathrm{yr}^{-1}$ and $\mathrm{SFR}_{IR}$=117 $M_{\odot}\mathrm{yr}^{-1}$. These objects are suspected to be recent mergers undergoing strong circumnuclear bursts of star formation that ionize the interstellar medium throughout the galaxy. Our Cold sample was not selected according to far-IR warmness as the Armus et al. sample, but it is directly comparable to it in terms of $L_{FIR}$ and $\alpha_{(25,60)}$. The ULFIRG sample ($L_{FIR} \geq 10^{12} L_{\odot}$) shows an even larger mean $\mathrm{SFR}_{IR}$=313 $M_{\odot}\mathrm{yr}^{-1}$. This is a sample of extremely bright, strongly interacting systems, their far-IR emission being associated with large scale star formation, triggered by the interaction.

Mazzarella etal. 1991 argued that the differences in IR properties (and SFRs) between these samples can be convincingly explained by invoking differing relative fractions and temperatures of the warm dust, increasing from 55% and $\mathrm{T}_d$=40 K for the Markarian sample to 80% and $\mathrm{T}_d$=50 K for the ULFIRGs sample. They suggested that there are possible correlations between *strong* encounters and increased far-IR emission, enhanced star formation and/or nuclear activity. This agrees with the conclusions that we reached earlier from our colour gradient data (see previous section) and is also consistent with the SFRs that we find for our sample objects: the Cold galaxies (mostly strongly interacting systems) show larger values by factors 2-3 compared to the Warm Seyfert sample. The four UL Warm Seyfert 2s with large IR luminosities and SFRs are also merging/interacting systems. The issue of interactions versus galactic ac-

tivity will be further explored in Paper V.

### 4.2. Colour-Colour Profiles

Colour-colour profiles have been commonly used in order to model the effects of dust and stellar populations (age-metallicity) in the colours of galaxies. Larson & Tinsley 1978 have shown that, while normal galaxies follow a well-defined relation ($(U-B)$ vs $(B-V)$ in their case), peculiar and interacting galaxies show a much larger scatter, with overall bluer colours. This difference was attributed to the latter having experienced anomalous SFRs, characterized by recent bursts. Several attempts to model galactic colours were put forward since then, the most sophisticated being stellar population synthesis models. Generally, there are several trends appearing in colour-colour diagrams: (a) The dispersion along the normal sequence indicates different rates of star formation, the colours becoming bluer for increasing SFR. However, metallicity (chemical composition) changes within a galaxy or among galaxies will have a similar effect on colours, that is, will move the colours parallel to the normal sequence, redder for higher metallicities. (b) The dispersion perpendicular to the normal sequence indicates differences in star formation bursts, the more recent (or shorter) bursts corresponding to bluer colours. However, another similar effect is produced by changing IMF, bluer colours being produced by more massive stars (flatter IMF). The degeneracy between these various factors is a major problem for the modeling of galaxy colours and gradients. Another major complication, is the degeneracy between stellar population and dust effects. IR data is very important for disentangling these effects and a variety of extinction models exist in the literature. De Jong 1996 computed extinction models for his sample of face-on spiral galaxies and found that the dust changes neither the shape of the disk light profiles (in his case exponential) or the colour gradients: varying the internal extinction produces only colour and surface brightness $\mu$ *offsets* (see also Bell & De Jong 1999). Similarly, for a sample of edge-on galaxies, Just etal. 1996 found that dust effects being constant in the optically thick central regions, do not affect the intrinsic colour gradients. They just *shift* their colours. If this is true in all galaxies it alleviates somewhat the degeneracy problem, providing that one is not interested in the absolute galaxy colours.

#### *4.2.1. Integrated Colours*

A large amount of exctinction must be present in all our sample galaxies. However, since we have no good measure for the internal exctinction and we are mainly interested in comparing the shapes (rather than the absolute values) of colour gradients between our objects, we shall not consider the effects of extinction in the discussion that follows. In Figure 9 we show $(B-R)$ vs $(V-R)$ plots for the Warm Seyfert 1 and 2 subsamples. The upper panels show integrated nuclear (filled dots) and disk (triangles) colours. The arrow indicates the Galactic extinction law for $A_V$=0.5 that, although an oversimplification of the real dust distribution, it is a gross indicator of the direction of dust exctinction effects (De Jong 1996). The nuclear and disk symbols are connected together to indicate aperture colour gradients (discussed in Section 3.1). Overplotted circles indicate the loci of integrated colours for a sample of face-on normal spirals (De Jong 1996), with morphological types T=0-10. The dashed line connecting smaller symbols represents the mean nuclear and disk colours for a sample of Markarian and NGC Seyfert galaxies (MacKenty 1990), which were found to possess in a large extent disturbed morphologies.

The first thing depicted here is the difference in the *sign* of the colour gradients between Seyfert 1 and 2 types, which was discussed earlier. The only two Seyfert 1s with a negative gradient (bluer disks) are faint objects (IRAS 04124-0803 and 13512-3731) and thus their location in this plot should be regarded with caution. Another immediate observation is that Seyfert 1s and 2s lie in different parts of the diagrams, the former having bluer colours than normal galaxies the latter mostly redder, this including both nuclear and disk (and thus integrated) colours. When computing differences between the mean *integrated* colours for our three subsamples and for the De Jong sample of normal spirals, we find that for all colours, except $(B-V)$, Seyfert 1s are bluer by $\sim$0.1-0.3 mag while Seyfert 2s (and Cold galaxies) redder by $\sim$0.05-0.2 mag. All our samples have $(B-V)$ colours that are bluer than normal galaxies. Although the magnitude of these differences is comparable to the colour errors given by De Jong 1996, they are consistent in sign for all the galaxies within our sample, indicating that the effect is real. The most likely interpretation is that the bluer colours of Seyfert 1s are due to contamination by the AGN, while the bluer $(B-V)$ colours in Seyfert 2s are due to strong star forma-

tion in their *disks* (their nuclear colours being redder than normal galaxy colours). A third observation is that the *nuclear* colours for each of the two Seyfert samples appear to lie along some type of sequence in Figure 9. We do not find this to be a sequence of Hubble types, interaction stage or of some other morphological peculiarity. In Paper II we have seen that the Warm Seyfert 1 nuclear colours scale with $\frac{L_{FIR}}{L_B}$. This was interpreted in terms of dust obscuration, which is likely to be represented by the sequence in the colour-colour plots. The trend for Seyfert 2 nuclei is more difficult to understand. There is one Seyfert 2 galaxy with apparently very blue $(V-R)$ colour; this is IRAS 13536+1836, a double nucleus system for which only the E nucleus is considered here (see also Paper II).

*4.2.2. Surface Colours*

Because integrated colours are usually dominated by the nucleus, a better approach is to use radial colour profiles, especially for the study of disk populations. In the lower panels of Figure 9 we plot the $(\mu_B - \mu_R)$ vs $(\mu_V - \mu_R)$ tracks starting from radius 2 kpc (filled circles) out to $\mu_B$=23 mag arcsec$^{-1}$ (triangles). The long-dashed lines on the Seyfert 2 plot indicate the double nucleus mergers IRAS 13536+1836 and 19254-7245. Not all objects plotted on the upper panels appear on the lower (those with shallow images were omitted). The distribution of points is similar between the upper and lower panels, but the tracks are quite different and will be discussed below in terms of comparison with population synthesis models. The dotted lines represent an average track for the normal spiral sample of De Jong 1996 for $0 \leq T \leq 5$, that is shifted towards bluer $(V-R)$ colours compared to both our Seyfert samples. For Seyfert 1s, the outer disk $(B-R)$ colours are quite similar to the spiral disk colours, while the inner $(B-R)$ colours are much bluer than the spiral nuclear colours. Seyfert 2s on the other hand have similar inner and outer disk $(B-R)$ colours with those of normal spirals, but significantly redder $(V-R)$ colours. Moreover, the Seyfert 2 tracks are often complex, due to additional components affecting their light profiles. De Jong has shown that all his galaxies have a negative gradient outwards that can be best explained by a combination of stellar age and metallicity effects, the outer parts being populated by younger and lower metallicity stars while the dust plays a minor role to the observed gradients. He also found a correlation between colours and surface brightness, both within and among galaxies, and a correlation between colours and morphological type T for the same surface brightness (see also Bell & De Jong 1999). As we have shown in Paper III, there is no significant correlation between morphological type and surface brightness (or any other disk parameter) in our samples. Neither do we find any correlations between colours or colour gradients and morphological type.

*Comparison with models*

In view of the age-metallicity-extinction degeneracy discussed in the previous section, we shall not attempt here to give an individual comparison between our data and stellar population synthesis models. Instead, we shall discuss the main trends for our sample objects using as reference some well-known population synthesis models, chosen to include both age and metallicity effects. In Figure 10 we split each sample into three (somewhat arbitrary) groups whose colour-colour tracks show some similarities. The left panels are reserved for Seyfert 1s, the right panels for Seyfert 2s. The population synthesis models are overplotted in each panel and decoded on the top left panel. Here is a short description of these models:

(i) Bica etal. 1990 (dotted line): Models of star forming events of the last $3\times10^9$ yr are superimposed on an old stellar populations. Here, young, low-metallicity star clusters are combined with the spectra of red strong-lined nuclei, to simulate the effects of starbursts induced by galaxy interactions, either through gas inflow from the disk to the nucleus of a spiral galaxy or through gas transfer from a spiral disk or irregular system to an earlier type galaxy. A library of observed star cluster spectra is used with IMF similar to those in starbursts. Three different models, labeled by 0.1%, 1% and 10%, are shown in Figure 10, representing the respective burst-to-old population mass fractions. The dots in all three models represent burst ages: $\leq$0.007, 0.02, 0.07, 0.2, 0.7, 2, 7 Gyr.

(ii) Worthey 1994 (dashed line): These models are calculated for a wide range of metallicities, but represent only a range of intermediate to old stellar populations: 1.5, 2, 3, 5, 8, 12, 17 Gyr. These are single-burst models using the standard Salpeter IMF with $0.1 \leq M \leq 2\ M_\odot$. In Figure 10 we show only the model corresponding to solar metallicity, mainly for comparison purposes with the other models presented here and because different metallicity tracks are almost su-

perimposed on each other for our plotted scales.

(iii) Bruzual & Charlot 1993 (dash-dotted line; see also Charlot & Bruzual 1991): Stellar population synthesis models, calculated for solar metallicities and starting from the very early stages of evolution: $\leq$0.0001, 2, 7, 12, 17 Gyr. These models use a Salpeter IMF with 0.1$\leq$M$\leq$100 $M_{\odot}$ and are calculated for different star formation histories, that is, a single burst, an exponentially declining SFR and a constant SFR model. On our plots we chose to represent the single burst model, for compatibility with the other models and also because this should be the most likely situation in Seyferts.

The Bruzual & Charlot and Worthey models are offset from each other (although the relative trends are similar), this being due to uncertainties in the used stellar evolutionary tracks (De Jong 1996). It was indeed found that large discrepancies exist between different population synthesis models, the uncertainties in stellar age for a given metallicity can be as large as 35% and in metallicity for a given age of the order of 25% (Charlot etal. 1996). That is, uncertainties in these two quantities are larger than any effects from changing IMFs or cut-offs. The main effects of model uncertainties are shifts in absolute colour values, but the predicted colour gradients and other relative trends within a galaxy or between different galaxies should be correct and directly comparable with the observations (see *e.g.,* De Jong 1996).

Let us now briefly discuss the main conclusions drawn from Figure 10. Throughout this discussion, the reader should be referring to the detailed colour profiles and two-dimensional maps shown in the Appendix of Paper III.

First of all, it is clear that our galaxies have very different profiles than those of normal spirals (shown as dotted line in Figure 9), which were better fitted by a combination of the Worthey and Bruzual & Charlot models (De Jong 1996).

(a) Upper panels: The Seyfert 1 galaxy on the left panel is IRAS 13512-3731 and the two Seyfert 2s on the right panel are IRAS 04507+0358 and 03202-5150. The first is a compact early-type galaxy; its nuclear blue colours are probably affected by the AGN and slightly reddened outwards through a track that is difficult to interpret given the large error bars. This object is redder than the rest of the Seyfert 1 sample; according to the Worthey or Charlot & Bruzual models, the indicated mean stellar ages are $\sim$5-8 Gyr. The first of the two Seyfert 2s mentioned above, IRAS 04507+0358, is also an early type galaxy whose colours lie within the above two sequences of models, indicating somewhat younger mean populations (within the model and data uncertainties) than the Seyfert 1 galaxy. The second Seyfert 2 galaxy, IRAS 03202-5150, is an early type galaxy, most likely interacting with a nearby companion. The main body has colours indicative of a relatively old stellar population (a mean of 5 Gyr according to the Worthey models). This galaxy has also a bar and ring features with associated star formation (see Appendix of Paper III), that are seen as loops in its colour profile and as a blue jump towards the loci of (star forming) models of Bica etal. 1990.

(b) Middle panels: The Seyfert 1 galaxies on the left panel are IRAS 02366-3101, 04493-6441 and 15015+1037. They are all isolated, early or intermediate type galaxies, with progressively redder colours in the cited order. They all have inverse (positive) gradients and their tracks are parallel and partially overlap with the Bica & Alloin tracks, indicating a very recent starburst (0.2-0.7 Gyr if the 10% model is to be used) superposed on an older stellar population. Given the size of the error bars, the colours could also fit the 1% model and a $\leq$0.1 Gyr starburst or, less likely, a Bruzual & Charlot model, with mean stellar ages $\sim$5 Gyr or younger.

The Seyfert 2 galaxies on the right panel are IRAS 03059-2309, 23254+0830, 02580-1136 and 20481-5715, this being a range of progressively redder mean colours. The latter is an early type galaxy with a nearby companion. There is little change in its colours, which show a 1-2 Gyr stellar population superposed on the redder underlying galaxy. IRAS 02580-1136 is an early-type barred spiral with strong star formation associated with its "grand design" spiral arms. Its colours are consistent with a young 10% starburst $\sim$1-2 Gyr old (or 0.1-0.2 Gyr if the 1% model is used), from disk to center. The other two Seyfert 2 galaxies are both later type spirals and members of strongly interacting systems. Both show grand design spiral arms (and tidal tails) with knotty star forming regions. Their colour profiles overlap with the 1% and 10% Bica et al. models, indicating recent star formation: 0.5-1 Gyr for the 10% model, or younger by a factor of 10 for the 1% model in IRAS 23254+0830 and 0.2-0.7 Gyr or younger in IRAS 03059-2309 (the range of stellar ages is from disk to center).

In summary, all the objects presented in these two

panels have colour profiles consistent with the evolutionary tracks of Bica et al. , but inconsistent with either of the other two models shown in Figure 10. Changes in metallicity would have only a minor effect (for instance may be responsible for the slightly differing slopes of the profiles), as it is apparent from the virtually overlapping Worthey models for a wide range of metallicities. The Charlot & Bruzual models for different star formation *histories* (not shown in Figure 10) do not resemble our colour profiles and lie far from our data points. Although the influence of the AGN makes it more difficult to interpret the Seyfert 1 inverse colour gradients, it is likely at least for the Seyfert 2s, that their colour gradients mainly represent stellar age effects, if extinction was to be ignored (dust extinction would have a similar effect on the colour profiles). Although for a simple Galactic exctinction law such an effect could not be much larger than $\sim$0.5 mag in $V$ band *within* a galaxy, different assumptions for the dust distribution could result in larger effects (*e.g.,* De Jong 1996 and references therein).

(c) Lower panels: In these plots we show objects with complex and unusual colour profiles that cannot be explained easily by a simple comparison with population models. The Seyfert 1s plotted in the left panel are IRAS 00509+1225, 23016+2221 and 21299+095. The first one (bluest of the three) is an early type spiral with knotty emission in its (one-sided) spiral arm. What makes it unusual is its very blue nuclear region. Its disk colours could be fitted with a very young starburst $\leq$0.5 Gyr old, superposed on the old galaxy population. IRAS 23016+2221 (with the bluest $(V-R)$ nuclear colour) is an object with peculiar morphology, reminiscent of a recent merger, originally given an early Hubble classification. Its strong H$\alpha$ emission within the central $\sim$5 kpc (see Appendix of Paper III) is probably responsible for the bluer $(V-R)$ disk compared to its nucleus. Modeling its colours with Bica & Alloin's tracks indicates a very young starburst of mean age 0.07-0.7 Gyr. The last object is IRAS 21299+095, an early type spiral which also shows strong circumnuclear H$\alpha$ emission, that causes its mean disk colours to become significantly bluer (compared to the nucleus). They can be fitted by a starburst of mean age 0.02-0.5 Gyr. It is difficult to explain its very red $(V-R)$ nuclear colour, though. On the right panel we show some extreme Seyfert 2 cases: IRAS 13144+4508, 11298+5313 (W and E members), 19254-7245 and 13536+1836 (in order of bluening $(V-R)$ nuclear colours). The first three objects have similar $(B-R)$ colours as the rest of the Seyfert 2 sample and their colour profiles are (roughly) following the evolutionary tracks of Bica & Alloin. However, their $(V-R)$ colours are strongly shifted to the red by $\sim$0.2-0.3 mag, distinguishing them from the rest of the sample. They are all members of multiple strongly interacting systems, suffering tidal distortions and they all have very blue $(B-V)$ (integrated) disk colours, indicating recent star formation events. They fit the description given by Larson & Tinsley 1978 of strongly interacting galaxies (at a particular stage of their dynamical evolution, involving tidal features), showing very blue $(B-V)$ colours, off the normal sequence in colour-colour plots. The latter two objects are examples of on-going mergers, with double nuclei embedded in a common body and large tidal tails extending radially outwards. Actually, the colours of IRAS 19254-7245 can be explained with a Bica & Alloin type of model, indicating starbursts with age $\sim$0.1-5 Gyr or younger if we allow for the (certainly very significant) dust effects, invoked in order to explain the steep colour gradient and the very red nuclear colour. On the other hand, it is very difficult to explain the colour profile of IRAS 13536+1836, part of the problem being the very blue W nucleus that affects the mean nuclear colour at 2 kpc.

We have not presented colour-colour profiles for any of the Cold sample objects. The only two objects among them with three-colour information are IRAS 07514+5327 and 06506+5025, both late-type barred spirals. On colour-colour diagrams as the ones of Figure 10, their colour profiles are similar to those of the third group Seyfert 2 galaxies (lower panels). They show very red colours that cannot be interpreted by any of the population synthesis models and their profiles vary almost perpendicular to the normal colour-colour sequence. These effects seem to be independent of the nuclear activity type (one object is a starburst, the other a Seyfert 1 galaxy).

We summarize our conclusions in the next section.

## 5. Conclusions

In this paper we have examined the colour distributions characterizing the host galaxies of our Warm and Cold samples. Our main conclusions are as follows:

1. The Warm Seyfert 1 galaxies show bluer nu-

clei and positive colour gradients, while the Warm Seyfert 2 and the Cold galaxies show the exact opposite trends. Most likely, these aperture gradients reflect the contamination of nuclear colours by the AGN in Seyfert 1s and by dust extinction in Seyfert 2s. In the Warm Seyfert 2 and Cold samples, the colour and emission line distributions are more complex than in the Warm Seyfert 1s, showing evidence for patchy dust extinction and intense star formation mostly associated with spiral and tidal features.

2. Surface colour gradients at radii $\geq$2 kpc, indicate a clear distinction between the Warm Seyfert 1 and 2 galaxies: For the Seyfert 1s, positive colour gradients persist even at large disk radii ($\geq$5 kpc) where contamination by the nucleus is minimal, most likely indicative of (increasing outwards) age gradients. In Seyfert 2s, any nuclear exctinction should not affect seriously the colour gradients at radii$\geq$2 kpc, which are thus dominated by (decreasing outwards) metallicity and stellar age effects. There is an overall similarity between Warm Seyfert 2 and Cold galaxy colour gradients, which indicates that similar (external) processes, such as strong interactions, must dominate their disk properties.

3. Seyfert 2 (bluer) colour gradients correlate with (larger) IR luminosities, indicating centrally concentrated dust and strong disk star formation. In fact, we find that both these observed quantities scale with interaction strength, a result that will be further explored in Paper IV.

4. The Cold sample shows larger SFRs (as deduced from their IR emission longword of 60 $\mu$m) by factors of 2-3 compared to the Warm Seyfert samples. However, if in the Seyfert 2 subsample we include the ultra-luminous ($L_{60} \geq 10^{11}$) (strongly interacting) members, it becomes statistically comparable to the Cold sample. Galactic interactions seem again to be the issue here, for the enhanced far-IR emission and SFRs.

5. The radial colour-colour profiles show that the Warm Seyfert 1 and Seyfert 2 galaxies occupy different regions (the first bluer, the second redder) in these diagrams. For each sample the galaxies can be grouped in three classes: (a) Early-type galaxies with mean disk stellar ages $\geq$5 Gyr (b) Early or intermediate-type galaxies with colours indicating starbursts $\sim$1 Gyr or younger, superposed on the older underlying galaxy population. Within this class, the Seyfert 1s are isolated objects while the Seyfert 2s are mostly interacting with a companion galaxy. (c) Objects with complex profiles and, in the case of Seyfert 2s, also complex morphologies. The Seyfert 1s are mostly single early-type systems with strong circumnuclear H$\alpha$ emission and colours indicating a very young starburst $\leq$0.5 Gyr superposed on the redder galaxy population. The Seyfert 2s in this class, are all extreme cases of strongly interacting, tidally distorted and double nucleus merging systems, that lie way off the normal sequence, with extremely red $(V-R)$ colours. The only two Cold galaxies with available three-colour information, belong also to this latter class of extreme profiles. We conclude that, for all three classes, the observed colour profiles can be described by age and dust effects within single-burst, solar metallicity models. Metallicity changes within or among the galaxies and differing star formation histories do not seem to affect significantly the above conclusions.

6. In double nucleus systems one of the two nuclei is activated and becomes the main source of optical and IR emission, ionizing the gas anisotropically. These characteristics are strikingly similar for the four mergers that we have observed, independently of which sample they belong to.

In the present Paper IV we have shown significant differences in the host Seyfert 1 and 2 colour distributions, that cannot be attributed to simple orientation effects. In turn, they seem to be related to the interaction stage of the host galaxy, at least for the Warm Seyfert 2 galaxies which in this respect are similar to the Cold galaxies. Through aperture photometry (Paper II) and decomposition of the host light profiles (Paper III) we have reached similar conclusions. In the forthcoming, last in this series, Paper IV we will combine all these results within the context of an evolutionary scenario for the Warm Seyfert galaxies.

I am grateful to my thesis advisors George Miley and Walter Jaffe for providing me with stimulation and support throughout the completion of this project. This research has made use of the NASA/IPAC Extragalactic Database (NED) which is operated by the Jet Propulsion Laboratory, California Institute of Technology, under contract with the National Aeronautics and Space Administration. Part of this work was completed while the author held a National Research Council - NASA GSFC Research Associateship.

## REFERENCES


Armus, L., Heckman, T.M., Miley, G.K. 1990, ApJ, 364, 471

Balcells, M., Peletier, R.F. 1994, AJ, 107, 135

Bell E.F., De Jong, R. 1999, astro-ph/9909402

Bica, E., Alloin, D., Schmidt, A. 1990, MNRAS, 242, 241

Bruzual, G.A., Charlot, S. 1993, ApJ, 405, 538

Bushouse, H.A., Werner, M.W. 1990, ApJ, 359, 72

Charlot, S., Worthey, G., Bressan, A. 1996, ApJ, 457, 625

Charlot, S., Bruzual, G.A. 1991, ApJ, 367, 126

Chatzichristou, E.T. 2000c, ApJ, *submitted* (Paper III)

Chatzichristou, E.T. 2000b, ApJ, *submitted* (Paper II)

Chatzichristou, E.T. 2000a, ApJ, *submitted* (Paper I)

Chatzichristou, E.T. 1999, PhD Thesis, Leiden University

Chatzichristou, E.T., Vanderriest, C. 1995, A&A, 298, 343

De Grijp, M.H.K., Keel, W.C., Miley, G.K., Goudfrooij, P., Lub, J. 1992, A&AS, 96, 389

De Grijp, M.H.K., Miley, G.K., Lub, J. 1987, A&AS, 70, 95

De Jong, R.S. 1996c, A&A, 313, 377

Devereux, N.A., Young, J.S. 1991, ApJ, 371, 515

Hunter, D.A., Gillet, F.C., Gallagher, J.S., Rice, W.L., Low, F.J. 1986, ApJ, 303, 791

Just, A., Fuchs, B., Wielen, R. 1996, A&A, 309, 715

Kennicutt, R.C.Jr., Tamblyn, P., Congdon, C.W. 1994, ApJ, 435, 22

Kennicutt, R.C.Jr. 1983, ApJ, 272, 54

Kotilainen, J.K., Ward, M.J. 1994, MNRAS, 266, 953

Larson, R.B., Tinsley, B.M. 1978, ApJ, 219, 46

MacKenty, J.W. 1990, ApJS, 72, 231

Mazzarella, J.M., Bothun, G.D., Boroson, T.A. 1991, AJ, 101, 2034

Mille,r G.E., Scalo, J.M. 1979, ApJS, 41, 513

Rieke, G.H., Loken, K., Rieke, M.J., Tamblyn, P. 1993, ApJ, 412, 99

Rieke, G.H., Lebofsky, M.J., Thompson, R.I., Low, F.J., Tokunaga, A.T., 1980 ApJ, 238, 24

Salpeter, E.E. 1955, ApJ, 121, 161

Scalo, J.M. 1986, Fund.Cos.Phys., 11, 1

Soifer, B.T., Boehmer, G., Neugebauer, G., Sanders, D.B. 1989, AJ, 98, 766

Vader, J.P., Vigroux, L., Lachieze-Ray, M., Sourivon, L. 1988, A&A, 203, 217

Wise, M.W., Silva, D.R. ApJ, 461, 155

Worthey, G. 1994, ApJS, 95, 107



This 2-column preprint was prepared with the AAS LaTeX macros v4.0.

TABLE 1
MEDIAN, MEAN AND DISPERSION OF THE APERTURE COLOUR GRADIENT DISTRIBUTIONS.

| | Seyf 1 | Seyf 2 | Cold | Seyf 1 | Seyf 2 | Cold |
|---|---|---|---|---|---|---|
| Quantity | $(B-V)_{disk-nucleus}$ | | | $(B-R)_{disk-nucleus}$ | | |
| Median | 0.175 | -0.300 | -0.015* | 0.125 | -0.330 | -0.115 |
| Mean | 0.092 | -0.374 | -0.015* | 0.112 | -0.304 | -0.186 |
| $\sigma$ | 0.223 | 0.275 | 0.310* | 0.310 | 0.215 | 0.311 |
| Quantity | $(V-R)_{disk-nucleus}$ | | | $(V-I)_{disk-nucleus}$ | | |
| Median | -0.025 | -0.020 | -0.090 | 0.305 | -0.100 | ··· |
| Mean | 0. | 0.042 | -0.060 | 0.285 | -0.093 | ··· |
| $\sigma$ | 0.169 | 0.234 | 0.175 | 0.277 | 0.204 | ··· |

*Few data points

TABLE 3
MEDIAN, MEAN AND DISPERSION OF THE SURFACE COLOUR GRADIENT DISTRIBUTIONS.

| | Seyf 1 | Seyf 2 | Cold | Seyf 1 | Seyf 2 | Cold |
|---|---|---|---|---|---|---|
| Quantity | | $\frac{\Delta(B-V)_I}{\Delta\alpha}$ | | | $\frac{\Delta(B-V)_O}{\Delta\alpha}$ | |
| Median | 0.082 | -0.059 | $\cdots$ * | 0.005 | -0.020 | 0.024* |
| Mean | 0.097 | -0.102 | $\cdots$ * | 0.004 | -0.035 | 0.024* |
| $\sigma$ | 0.033 | 0.143 | $\cdots$ * | 0.011 | 0.061 | 0.041* |
| Quantity | | $\frac{\Delta(B-R)_I}{\Delta\alpha}$ | | | $\frac{\Delta(B-R)_O}{\Delta\alpha}$ | |
| Median | 0.110 | -0.079 | -0.045 | 0.011 | -0.012 | -0.002 |
| Mean | 0.116 | -0.083 | -0.005 | 0.011 | -0.029 | -0.010 |
| $\sigma$ | 0.050 | 0.073 | 0.114 | 0.013 | 0.068 | 0.013 |
| Quantity | | $\frac{\Delta(V-R)_I}{\Delta\alpha}$ | | | $\frac{\Delta(V-R)_O}{\Delta\alpha}$ | |
| Median | 0.041 | -0.001 | -0.020* | -0.003 | -0.004 | -0.027* |
| Mean | 0.027 | 0.021 | -0.405* | -0.005 | -0.008 | -0.027* |
| $\sigma$ | 0.052 | 0.081 | 0.028* | 0.013 | 0.017 | 0.028* |

| Break (kpc) | | | |
|---|---|---|---|
| | Seyfert 1 | Seyfert 2 | Cold |
| Median | 5 | 4 | 3.5 |
| Mean | 4.9 | 4.3 | 4 |
| $\sigma$ | 1.5 | 1.6 | 1.6 |

*Few data points

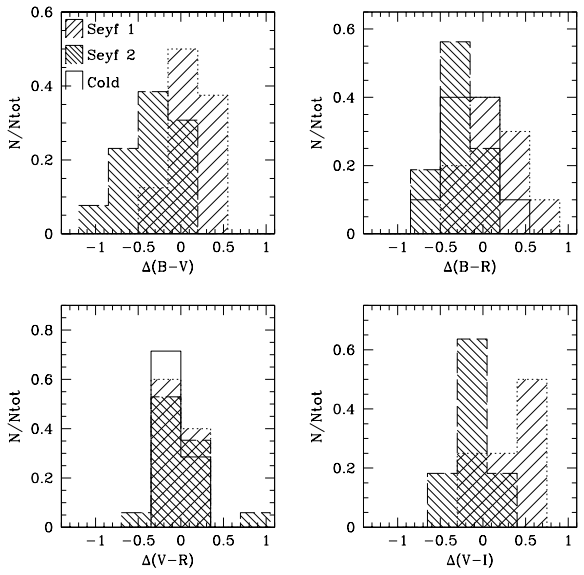


Fig. 1.— Distributions of colour gradients, obtained from aperture (disk)-(nuclear) colours, for our three samples. On the $\Delta(B-V)$ and $\Delta(V-I)$ histograms the Cold sample is not shown, due to the small number of data points.

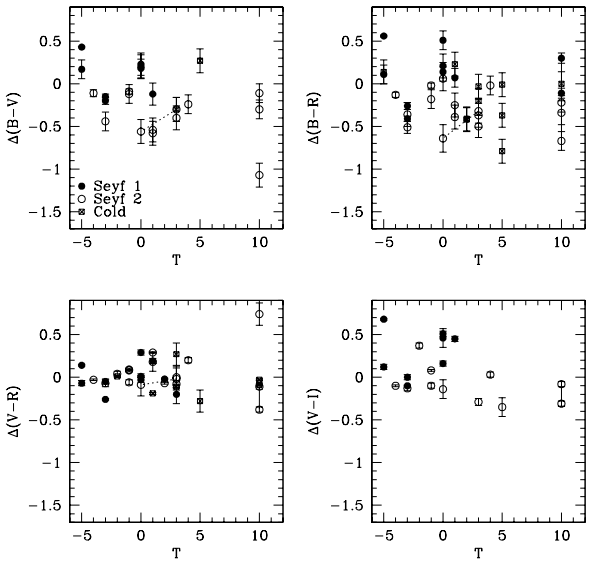


Fig. 2.— Colour gradients obtained from aperture (disk)-(nuclear) colours versus morphological type T. T=10 is conventionally used for highly disturbed or double nucleus merger systems. Full lines connect members of an interacting system that are the possible IRAS candidates. Dashed lines connect the two nuclear colours of double nucleus merger systems.

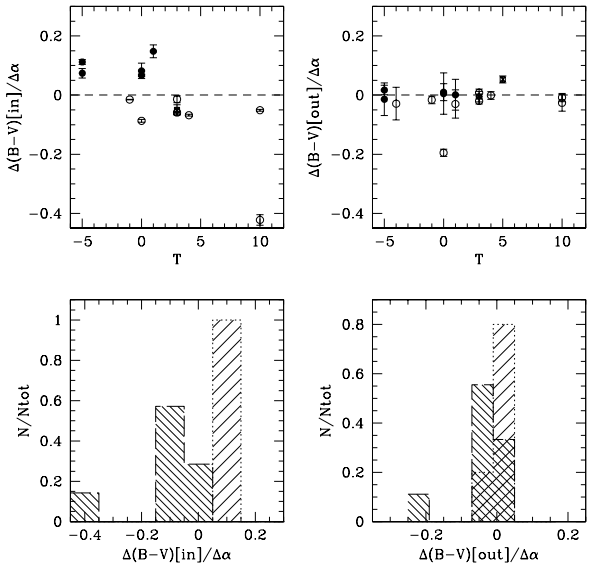


Fig. 3.— Disk surface $\mu_B - \mu_V$ *inner* and *outer* colour gradients (obtained as described in the text). Upper panels: versus morphological type T (symbols as in Figure 2). Lower panels: distributions for the Seyfert 1 and 2 samples (symbols as in Figure 1).

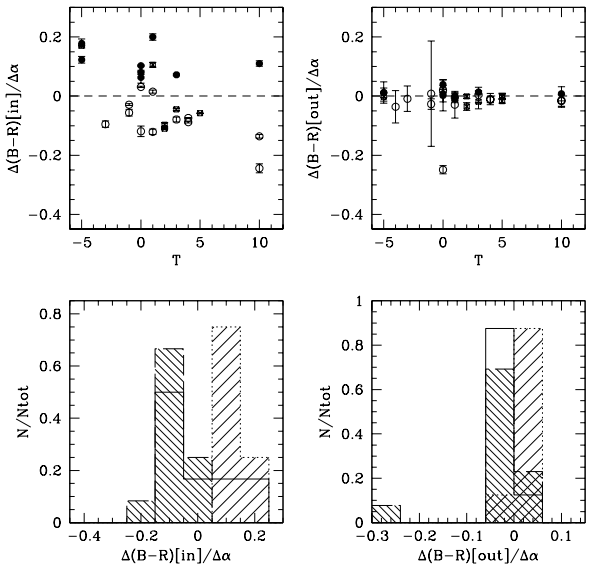


Fig. 4.— Disk surface $\mu_B - \mu_R$ *inner* and *outer* colour gradients (obtained as described in the text). Upper panels: versus morphological type T (symbols as in Figure 2). Lower panels: distributions for the three (sub)samples (symbols as in Figure 1). (The Seyfert 2 galaxy that shows the atypically large error bar in its outer $(B - R)$ gradient is IRAS 03202-5150, due to its faint $B$ image).

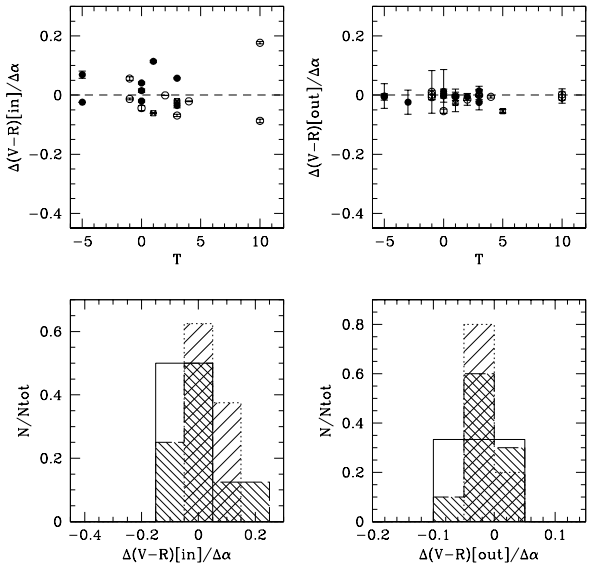


Fig. 5.— Disk surface $\mu_V - \mu_R$ *inner* and *outer* colour gradients (obtained as described in the text). Upper panels: versus morphological type T (symbols as in Figure 2). Lower panels: distributions for the three (sub)samples (symbols as in Figure 1).

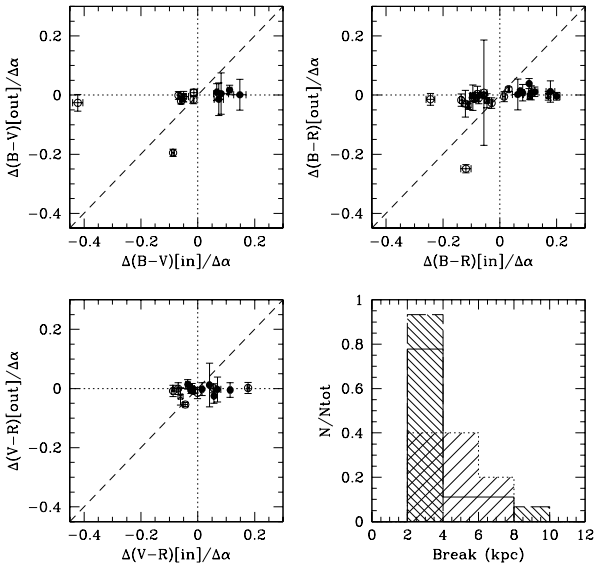


Fig. 6.— *Inner* versus *outer* disk surface colour gradients (obtained as described in the text; symbols as in Figure 2). The long-dashed line indicates the line of equal colour gradients. The lower right panel shows the distribution of the radii where the break in colour profiles occur, for the three (sub)samples (symbols as in Figure 1).

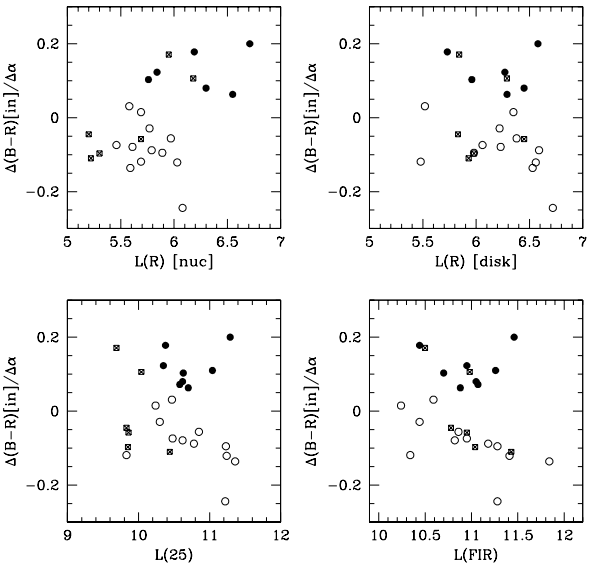


Fig. 7.— Disk surface colour gradients versus optical and IR luminosities (in units of $\log(L_{\odot})$; the errors associated with the data points were omitted here for clarity; symbols are as in Figure 2).

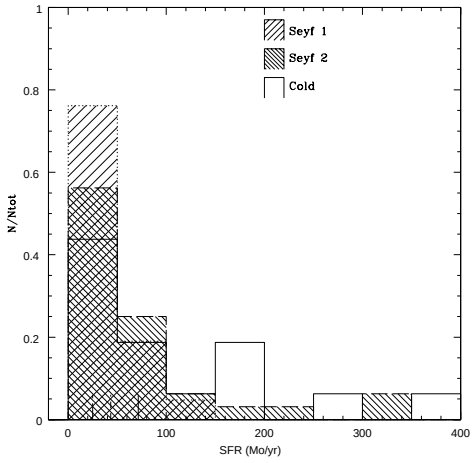


Fig. 8.— Distribution of star formation rates obtained from far-IR emission for our samples. The vertical bars on the lower x-axis indicate median values for each sample: long-dashed bar for Seyfert 1s, short-dashed for Seyfert 2s and full-line bar for the Cold sample.

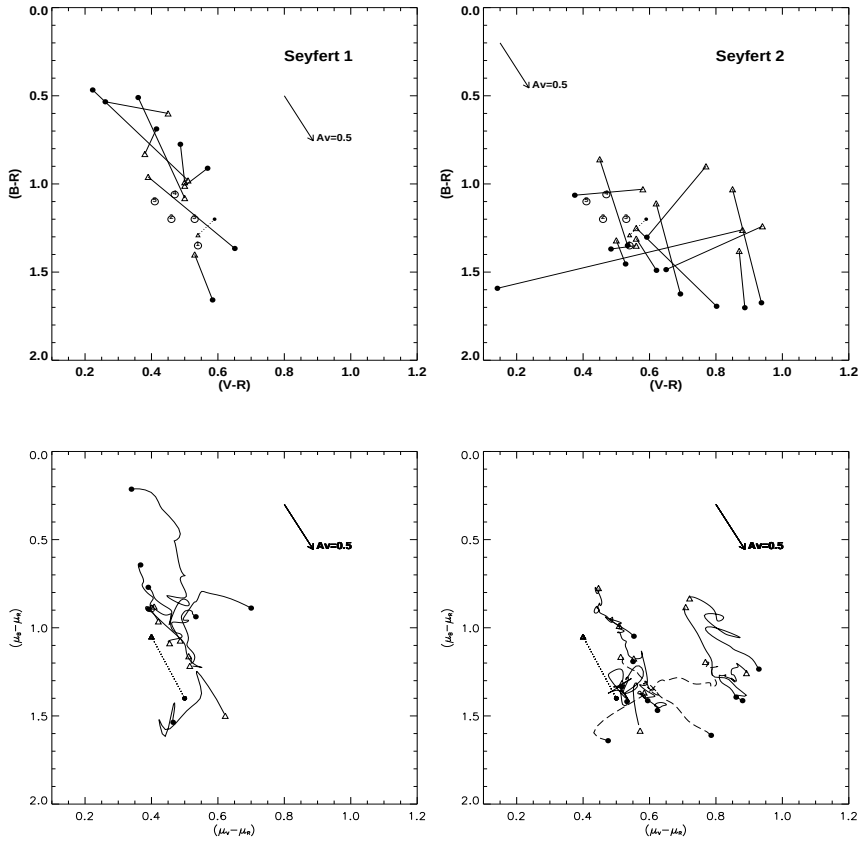


Fig. 9.— Upper panels: Aperture $(B-R)$ colour-colour plots; filled circles are nuclear and triangles disk colours. The arrow indicates the Galactic extinction law. The circles indicate the loci of *integrated* colours for a sample of face-on normal spirals (1:T=0-2, 2:T=2-4, 3:T=4-6, 4:T=6-8. 5:T=8-10; De Jong 1996).The dashed line and smaller symbols indicate average colours for the Seyfert sample of MacKenty 1990. Lower panels: Surface $(B-R)$ colour-colour plots, left panel Seyfert 1s, right panel Seyfert 2s; filled circles are colours at 2 kpc from the nucleus and triangles correspond to colours at the $\mu_B$=23 mag arcsec$^{-1}$ isophote. The dashed line indicates an average profile for normal spirals (above reference) and the long-dashed lines in the Seyfert 2 plot indicate the tracks of double nucleus merger systems.

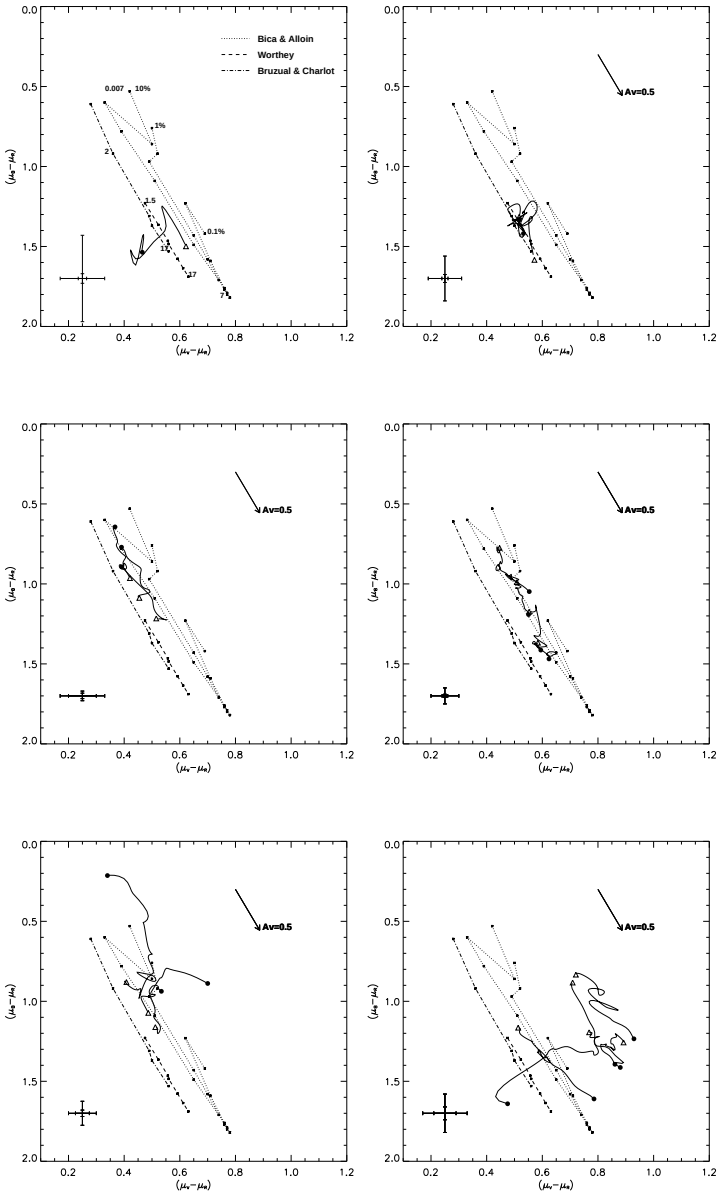


Fig. 10.— Surface $(V-R)$ vs $(B-R)$ colour-colour plots (full lines): left panels for Seyfert 1s right panels for Seyfert 2s. Filled circles are colours at 2 kpc from the nucleus and triangles correspond to colours at the $\mu_B$=23 mag arcsec$^{-1}$ isophote. Population synthesis models are overplotted, the coding given in the upper left panel. The small dots within each model represent stellar ages with the younger and older labeled in units of Gyr (the full range is given in the text). The % labels in the three Bica & Alloin models represent burst-to-old population mass fractions. The arrows indicate a standard Galactic extinction law. Error bars plotted on the lower left corner indicate the average inner (smaller) and outer (bigger) errors for the objects in that panel.